Sensors & Diagnostics

PAPER

View Article Online
View Journal

Cite this: DOI: 10.1039/d5sd00228a

A carbohydrate-based graphene field-effect transistor sensing system for rapid blood type detection

Yunqing Li, * Pengyu Li, Yiping Yao and Weiwen Zhao

Received 16th December 2025,
Accepted 8th May 2026

DOI: 10.1039/d5sd00228a

rsc.li/sensors

Blood typing is essential in fields such as blood transfusion, organ transplantation and forensic identification. Traditional blood typing methods are usually time-consuming, operationally complex, and reliant on large-scale laboratory equipment, limiting their application in point-of-care testing. Therefore, the development of a rapid and portable blood typing method is of great significance for clinical diagnosis and emergency medical care. In this work, we develop a novel dual-channel carbohydrate-based graphene field-effect transistor (C-GFET) sensing system to achieve rapid ABO blood typing. By functionalizing the graphene surface with aminated antigen trisaccharides, the system enables the detection of blood type markers in real serum samples and determines the blood type based on the detection results. The results demonstrate that the device can specifically distinguish different blood type samples, offering a promising new strategy for point-of-care blood typing.

1. Introduction

The blood group system is the collective designation for specific antigens on the membrane of red blood cells, among which the ABO blood group system is the earliest discovered and holds great significance.[1] Accurate and rapid blood typing plays an irreplaceable role in preventing hemolytic transfusion reaction, guiding organ transplant compatibility and facilitating forensic individual identification. Traditional blood typing methods, such as the slide agglutination test and column agglutination technique, are usually time-consuming, operationally complex, and reliant on large-scale laboratory equipment, limiting their application in point-of-care testing (POCT).[2] Consequently, the development of novel, rapid, portable, and low-cost blood typing technologies has remained a focal point of research.

In recent years, biosensor technology has demonstrated great application potential in clinical diagnosis, environmental monitoring and food safety due to its advantages of high sensitivity, high specificity, rapid response, and ease of miniaturization.[3–6] In blood type detection, researchers have attempted to construct blood type sensors by Electrochemical technology,[7–12] quartz crystal microbalance (QCM)[13] and surface plasmon resonance (SPR).[14,15] However, these methods still face challenges in practical applications, including the cumbersome probe modification process of electrochemical methods; the lack of specificity in the QCM method; and the susceptibility of the SPR method to environmental interference.[16]

To enhance the performance of the sensors, various nanomaterials such as graphene,[17–20] carbon nanotubes,[21,22] metal nanoparticles and quantum dots[23,24] have been widely employed as sensitive elements, as their large specific surface area,[25] high electron mobility,[26] and ease of surface functionalization endow the sensors with high sensitivity and low detection limits.[27]

By immobilizing probes on the surface of sensitive materials such as graphene, the sensors can acquire specific recognition capabilities. Upon specific binding with the target, the spatial conformation of the probe changes, and the sensing system transduces this change into an observable electrical signal,[3,28,29] thereby achieving target detection. Therefore, a highly sensitive and selective blood typing sensing system can be constructed by this method. Furthermore, portable blood type testing devices are particularly important for enabling rapid point-of-care blood typing.[30]

The key factor for differentiating different blood types lies in detecting whether anti-A and anti-B antibodies exist in the serum. (Fig. 1a).[31,32] Serum from type A blood contains only B antibodies, type B serum contains only A antibodies, type AB serum contains neither,[33] and type O serum contains both[34] (Fig. 1b). Based on this characteristic, this study develop a dual-channel carbohydrate-based graphene field-

Shanghai Technical Institute of Electronics and Information, Shanghai 201512, China. E-mail: 18916550896@163.com

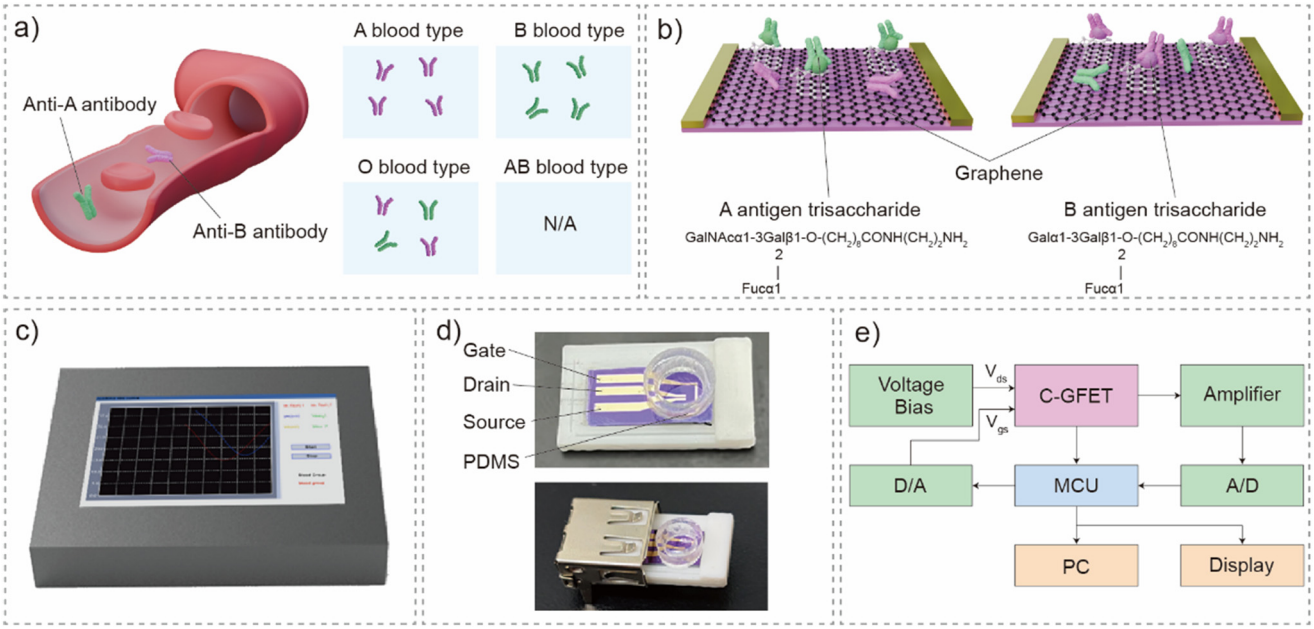

Fig. 1 a) Types of antibodies contained in ABO blood type blood. b) C-GFETs modified with aminated A antigen trisaccharides and aminated B antigen trisaccharides to simultaneously detect antibody types. c) Display of the handheld device. d) Physical appearance and composition of the C-GFET. e) Block diagram of the device control system.

effect transistor (C-GFET) sensing device that enables the simultaneous detection of two blood group-related targets (A antibodies and B antibodies) in serum by modifying A antigen trisaccharides and B antigen trisaccharides on graphene channel (Fig. 1c–e). In this study, the GFET structure is optimized by eliminating the bulky and expensive external reference electrode, enabling the integration of GFET arrays on a silicon substrate. Through the photolithography and metal thermal evaporation deposition systems, large-scale production of GFETs can be achieved, significantly reducing the cost per test. Additionally, we design a corresponding portable signal readout device, establishing the key technological foundation for transitioning from laboratory research to large-scale manufacturing. This system achieves the simultaneous detection of multiple targets and the determination and output of multiple results, thereby promoting the development of integrated bio-sensing technology and its clinical application.

2. Methods

The graphene surface is functionalized *via* π–π stacking interactions using 1-pyrenebutanoic acid succinimidyl ester (PASE). The pyrenyl moiety of PASE spontaneously adsorbs onto the graphene lattice, while its *N*-hydroxysuccinimide (NHS) ester group provides a reactive handle for biomolecular conjugation. Blood group-specific antigen trisaccharides (A/B types) are chemically engineered with terminal amino groups. These amines undergo nucleophilic addition to the PASE-NHS ester, forming stable amide bonds. This covalent linkage orients the antigen's glycan epitopes outward, preserving their recognition capability against serum antibodies. Immobilized antigens introduce n-type doping to graphene, evidenced by a negative shift in the Dirac point voltage (V_{Dirac}). This arises from the intrinsic negative charge of glycosylated structures, which electrostatically gates the graphene channel *via* field-effect coupling.

2.1. Materials

Antibody HE-193 (anti-blood group A antigen antibody), antibody HEB-29 (anti-blood group B antigen antibody) were purchased from Abcam. Aminated blood group A antigen trisaccharide, aminated blood group B antigen trisaccharide was purchased from Dextra.

2.2. Fabrication of the graphene field-effect transistor

Photoresist LOR 3A was spin-coated onto a silicon wafer (1 min, 3500 rpm). The coated wafer was heated at 175 °C for 300 s, cooled, and then spin-coated with photoresist AZ 1512 (1 min, 4000 rpm), followed by heating at 110 °C for 120 s. The wafer was exposed using a mask aligner (60 W m^{-2}, 3.4 s), developed for 35 s, rinsed with water, and dried with nitrogen. Chromium (20 nm) and gold (40 nm) were sequentially deposited using an evaporator. The wafer was then immersed in Remover PG for 8 hours to strip the photoresist. Fig. S1a) illustrated the preparation process of gold electrodes.

Graphene grown on copper foil was cut into 5 × 5 mm^2 pieces and floated on APS (4%) solution for 3 h to etch the copper. The graphene was transferred to deionized water for 1200 s, then onto gold electrodes, and left in a vacuum chamber for 5 h. After heating at 180 °C for 1 h, the sample was immersed in acetone for 3–4 h to remove polymethyl

methacrylate (PMMA), rinsed with isopropanol and deionized water, and dried with nitrogen. Fig. S1b) illustrated the PMMA-mediated graphene transfer method.

2.3. Graphene Channel functionalization

PASE was dissolved in DMF to prepare a 5 mM solution. The GFET was immersed in PASE solution for 3 h, rinsed with DMF for 15 min, and then washed with ethanol and deionized water before drying with nitrogen. The graphene field-effect transistor was then incubated in 10 μM aminated A or B antigen trisaccharide solution (in PBS) for 12 h, rinsed with phosphate buffer, and dried with nitrogen.

2.4. Portable electronic device circuit design

The chips TPS62913, AMS1117-3 V3, AMS1117-1 V8, and REF5025 were selected to provide the required voltages for different parts of the portable electronic device. The main MCU was STM32F429IGT6, the operational amplifier was LT1462ACS8, the D/A module used DAC8831, the A/D data acquisition used ADS1274, and the FT232R chip was used to convert UART signals from the device MCU into USB signals

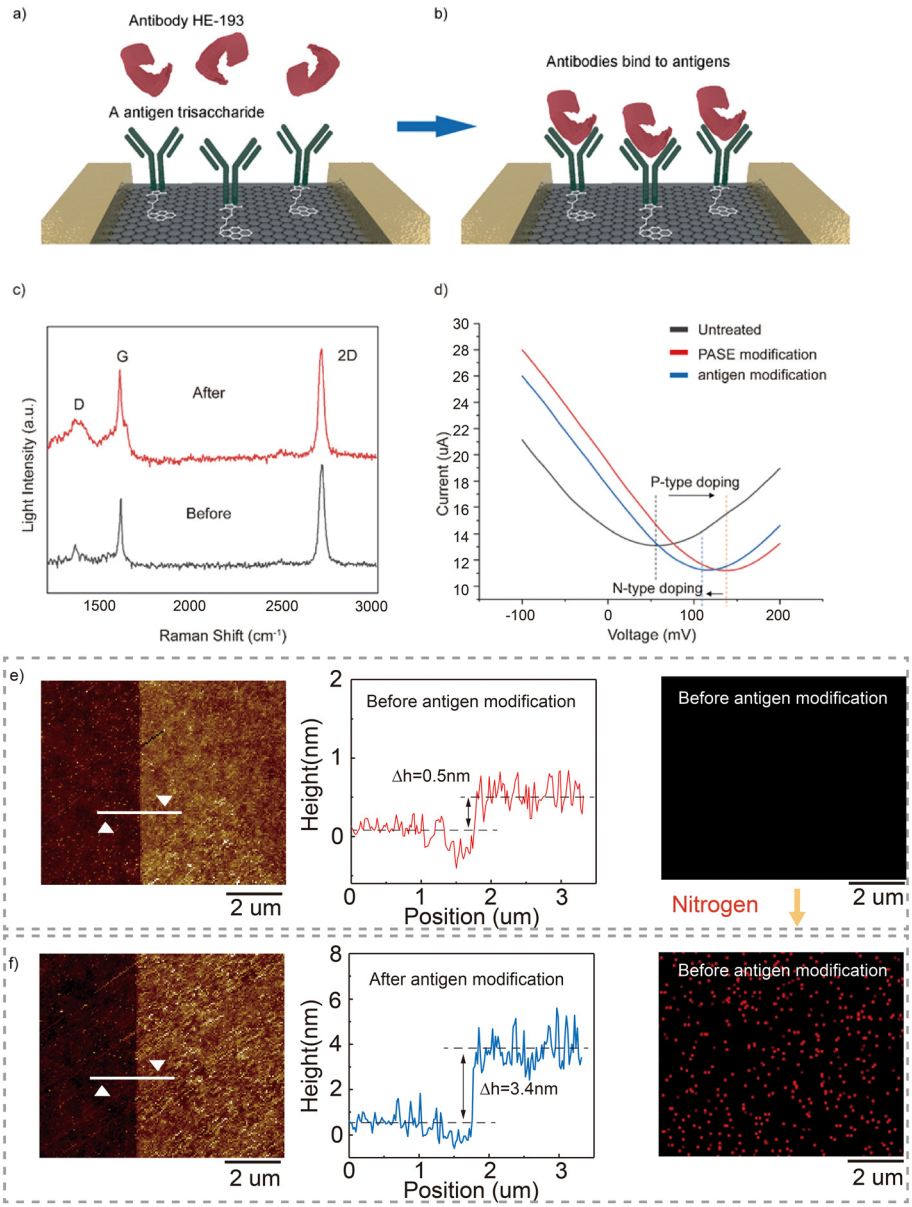

Fig. 2 Antigen–antibody binding process and characterization of graphene before and after functionalization. a) A antigen trisaccharide immobilized on the graphene surface and free antibody HE-193 in solution. b) A antigen trisaccharide on the graphene surface captures antibody HE-193 and forms a stable structure. c) Raman spectra of graphene before and after PASE modification. d) Transfer characteristics of graphene before PASE modification (untreated), after PASE modification and after aminated antigen trisaccharide modification. e) AFM and EDS characterization of graphene before antigen modification. f) AFM and EDS characterization of graphene after antigen modification.

for transmission to the host computer. The touch display module used a capacitive touchscreen, model G917S.

2.5. Real serum sample collection

All experiments using human serum samples were performed in accordance with the Ethical Guidelines for Biomedical Research Involving Human Subjects of the People's Republic of China, and approved by the Ethics Committee of Shanghai Technical Institute of Electronics and Information. Informed consents were obtained from human participants of this study. The process for obtaining serum samples in this study is as follows: the test subject's fingers are disinfected using an alcohol swab, and then the finger is pricked with a blood collection needle. Pressure is applied to the pricked area to extract blood, and 4–5 μL of blood is collected using a micropipette. The blood sample is then transferred to a pre-prepared tube containing 200 μL of PBS and thoroughly shaken to ensure uniform mixing. The mixture is subsequently placed in an environment at 3–5 °C for 30 minutes until the diluted blood separates into layers. The supernatant is then collected using a micropipette, transferred to another tube, and stored at low temperature for subsequent use. The process for obtaining real serum samples was shown in Fig. S2.

3. Results and discussion

3.1. Characterization

The detection mechanism takes advantage of the specific antigen–antibody recognition inherent to the ABO blood group and is converted into a quantifiable electronic signal by graphene field effect modulation. Firstly, PASE is immobilized on the surface of graphene by π–π stacking interactions. Secondly, the antigen trisaccharides functionalized with amino groups are condensed and immobilized on the surface of graphene by amidation reaction, so as to complete the functionalization of graphene. Here, the binding process of antigen trisaccharide fixed on graphene and antibody HE-193 is used as an example to introduce the principle of achieving blood group discrimination. As shown in Fig. 2a, initially, the antibody HE-193 was in a free state, while the A antigen trisaccharide was fixed on the graphene surface by PASE. Further, as shown in Fig. 2b, when the A antigen trisaccharide captured the free antibody HE-193, the two would undergo a specific antigen–antibody binding, quickly curling into a stable and compact structure. This specific binding process would bring the target molecule closer to the graphene surface, shortening the distance between the target molecule and the graphene surface to a few nm. The negatively charged antibody complex (with a physiological pH value of pH ~5–7) will, in order to maintain the electrical field balance, induce opposite charges to the antibody complex under the contact surface of the graphene and the solution, and the positive charges on the other side of the solid–liquid contact surface will also undergo an equal change at the corresponding position. This causes an equal increase in the number of freely mobile electrons within the graphene due to the charge conservation within the graphene, thereby changing the Dirac point voltage position of the graphene. We set two parallel groups of sensing devices modified with A and B antigens respectively, and used these two parallel sensing devices for simultaneous detection. Since each device was only modified with one antigen, different blood types would result in different Dirac point movements. By comparing the changes in the Dirac point movement of the two sensing devices, we can achieve the differentiation of A, B, AB, and O blood types.

To verify the successful modification of PASE on the graphene surface, Raman spectra of the graphene surface before and after PASE modification were measured. The results are shown in Fig. 2c: The selected diffraction range was 1200–3000 cm^{-1}. Before PASE modification, two distinct peaks were observed at approximately 1596 cm^{-1} and 2695 cm^{-1}, corresponding to the G and 2D peaks of graphene. Since intrinsic graphene is a zero-bandgap semiconductor, PASE modification affects it by opening the bandgap. The D peak is related to defects during Raman diffraction, and its intensity can serve as an indicator of successful PASE modification. A significant change in the intensity of the D peak at 1224 cm^{-1} before and after PASE modification confirmed the successful modification of PASE on the graphene surface.

Additionally, we measured the transfer characteristic curves of the GFET before PASE modification, after PASE modification, and after aminated antigen trisaccharide modification. The results (Fig. 2d) showed that after PASE modification, the transfer curve exhibited a significant right shift, with the Dirac point (the lowest point of the curve) gate voltage V_{Dirac} increasing by 81 mV. This indicated that PASE modification reduced the number of electrons in graphene, introducing p-type doping. After antigen modification, the transfer curve shifted left, and the Dirac point gate voltage decreased by 21 mV, indicating the introduction of n-type doping due to electron donation. This can be explained by the fact that while the pyrene structure acts as an electron donor, the *N*-hydroxysuccinimide group attached to it is an electron acceptor with stronger electron-attracting ability. Thus, when in contact with the graphene surface, the result was a reduction in the number of mobile electrons in graphene. On the other hand, aminated antigen trisaccharides are typically negatively charged in solution. When connected to PASE and brought close to graphene, their negative charges introduced n-type doping into graphene through electrostatic induction. These changes in electrical signals confirmed the successful modification of PASE and aminated antigen trisaccharides. Furthermore, AFM and EDS analyses revealed that after the graphene was modified with the antigen (Fig. 2e and f), the average height increased from 0.5 nm to 3.4 nm, and nitrogen elements appeared on the surface. These changes in electrical signals

confirmed the successful modification of PASE and aminated antigen trisaccharides.

3.2. Blood type detection

To verify the ability of the antigens modified on the graphene surface to recognize antibodies in the detection environment, anti-A antibody and anti-A antibody were diluted 20-fold with 1× PBS to simulate the antibody environment in real human serum. Aminated A antigen trisaccharides and aminated B antigen trisaccharides were modified onto the graphene surface. Then, 20 μL of the diluted anti-A solution was added dropwise to both the C-GFETs (aminated A antigen trisaccharide) and unmodified GFETs, 20 μL of the diluted anti-B solution was added dropwise to both the C-GFETs (aminated B antigen trisaccharide) and unmodified GFETs. After 8 min of stabilization, the transfer characteristic curves of graphene were measured. The results are shown in Fig. 3a. The V_{Dirac} of the transfer curve for the C-GFET modified with aminated A antigen trisaccharides shifted by 25 mV, while the unmodified GFET shifted by only 4 mV. The V_{Dirac} of the transfer curve for the C-GFET modified with aminated B antigen trisaccharides shifted by 31 mV, while the unmodified GFET shifted by only 5 mV. This proved that the C-GFET could recognize human blood group antibodies.

The statistical results obtained from the test in the PBS environment are presented in Fig. 3b. Test group 1 was a PBS solution containing anti-A antibodies, simulating type B serum. When the test solution containing anti-A antibodies was added dropwise to both the aminated A antigen trisaccharide-modified and aminated B antigen trisaccharide-modified C-GFETs, the former exhibited a larger Dirac point shift. By comparing the changes in Dirac point gate voltage between the two sensing devices, type B blood could be clearly distinguished. Similarly, test group 2 was a PBS solution containing anti-B antibodies, simulating type A serum. The aminated B antigen trisaccharide-modified C-GFET exhibited a larger Dirac point gate voltage change for this test solution. The above experimental results demonstrated that a device group composed of C-GFETs

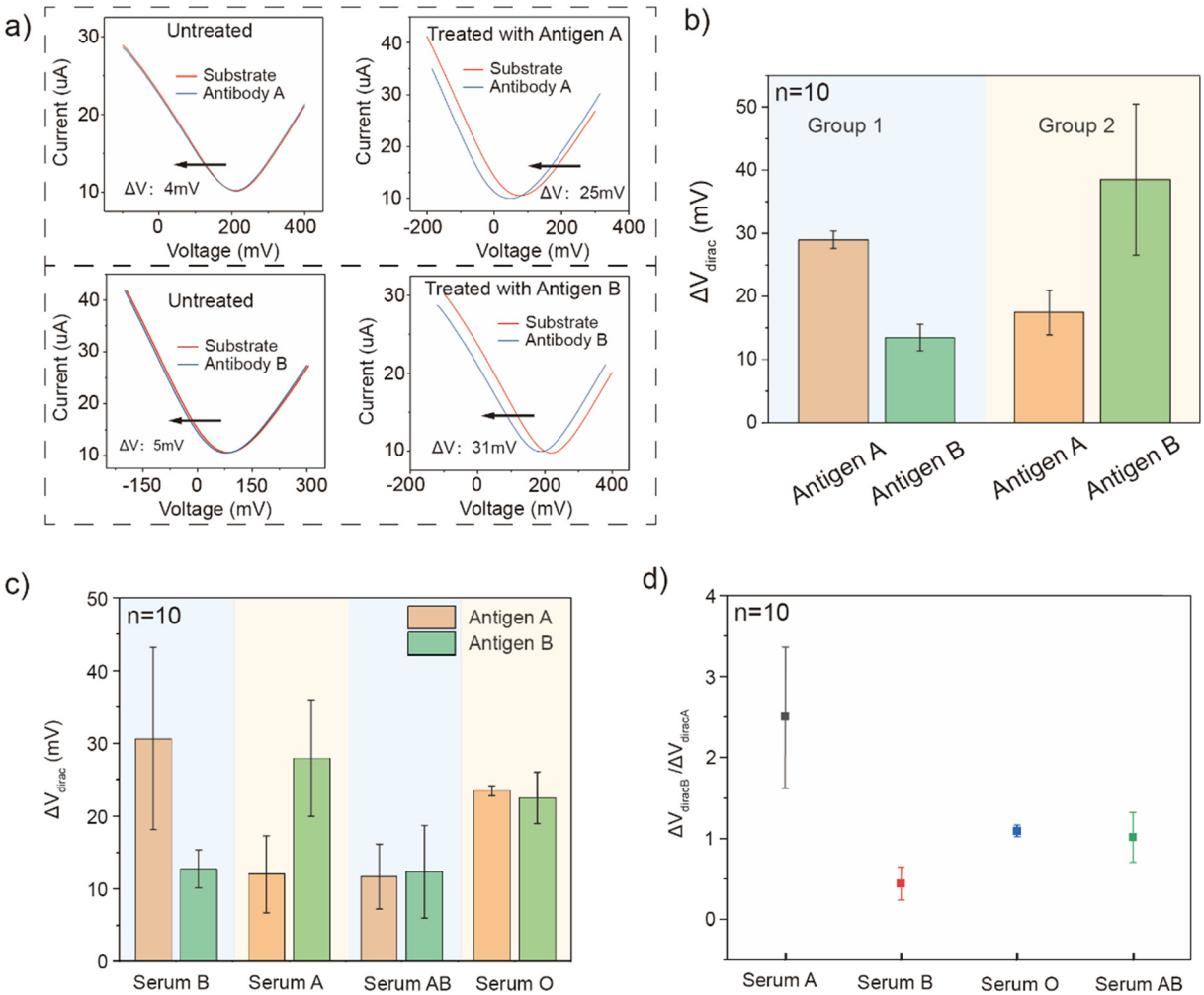

Fig. 3 a) Modified blood group antigen trisaccharide and unmodified graphene sensor transfer characteristic curve; b) Dirac voltage of the C-GFET in simulated serum B (group 1) and simulated serum A (group 2); c) specificity validation of C-GFET for real serum detection; d) ratio of ΔV_{DiracB} (B-antigen trisaccharide-modified C-GFET) to ΔV (A-antigen trisaccharide-modified C-GFET) across experimental groups.

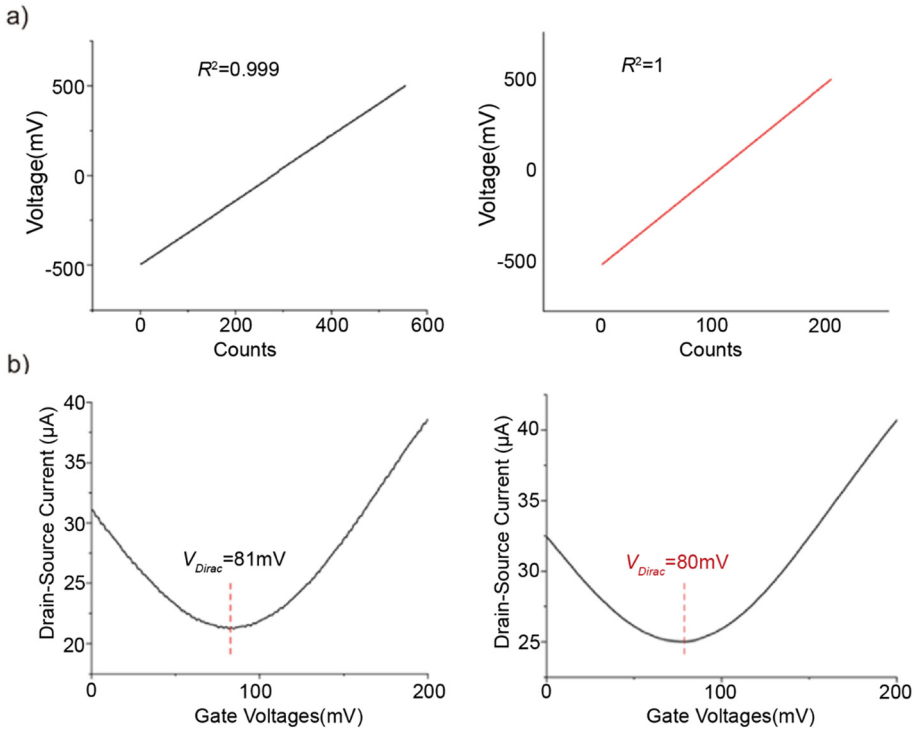

Fig. 4 a) C-GFET device step gate voltage (−500 mV∼+500 mV) measurement value; b) comparison of portable device and source meter measurement data for the same GFET transfer characteristic curve.

modified with A and B antigen trisaccharides could successfully identify simulated type A and B sera. To characterize device variability and stability, we measured the temporal evolution of the Dirac point voltage shift for different C-GFETs in PBS, as detailed in Fig. S3. The results indicate that after 1, 3, 7, and 14 days, the Dirac point voltage shifts of the tested devices remained consistently near zero, demonstrating excellent device stability and minimal device-to-device variation.

Subsequently, we tested four types of real serum samples (A, B, AB, O) using a device group consisting of two C-GFETs modified with A and B antigen trisaccharides. The results are shown in Fig. 3c: For type A serum, which contains only anti-B antibodies, the average Dirac point gate voltage shift for the B antigen trisaccharide-modified C-GFET was 28 mV, greater than the 12 mV for the A antigen trisaccharide-modified C-GFET. Similarly, for type B serum, which contains only anti-A antibodies, the A antigen trisaccharide-modified C-GFET exhibited a larger average Dirac point gate voltage shift of 30.67 mV, compared to only 12.75 mV for the B antigen trisaccharide-modified C-GFET. For type O serum, which contains both anti-A and anti-B antibodies, both C-GFETs responded, with average Dirac point gate voltage shifts of 23.5 mV and 22.5 mV, respectively. For type AB serum, which contains neither antibody, the Dirac point gate voltage shifts for both C-GFETs were small, at 11.67 mV and 12.33 mV, respectively. The experimental results demonstrated that the C-GFETs prepared in this paper could distinguish the ABO blood types of real sera. To further validate the detection specificity of the sensing device, we selected other biomarkers present in serum—including C-reactive protein (CRP), immunoglobulin (IgG), interleukin-6 (IL-6), and interferon γ (IFN-γ)—as targets. We measured the signal responses of both the A antigen trisaccharide-modified sensing device (Fig. S4) and the B antigen trisaccharide-modified sensing device (Fig. S5) to these biomolecules in PBS buffer. The results presented in the revised SI, confirm that the proposed sensing device exhibits excellent detection specificity.

The blood type determination criteria are established by integrating the detection results from the two channels functionalized with A and B antigens, respectively. For AB-type serum, which contains neither A nor B antibodies, the distinguishing feature from other blood types is the relatively weak detection signals obtained from both channels. The sum of the maximum signals from the two channels served as the criterion for differentiating AB-type serum from other types, with a threshold signal of 29 mV (calculated as the sum of the mean values and standard deviations of the two channel signals). Specifically, a sum of the two-channel detection signals below 29 mV indicates AB blood type, while values exceeding this threshold require further differentiation. As illustrated in Fig. 3d, the ratio $\Delta V_{\mathrm{DiracB}}/\Delta V_{\mathrm{DiracA}}$ can be used to distinguish between A, B, and O blood types. The lower deviation limit of the detection results for A-type serum ($\Delta V_{\mathrm{DiracB}}/\Delta V_{\mathrm{DiracA}}$ = 1.6) was established as the boundary between A and O blood types, while the upper deviation limit for B-type serum

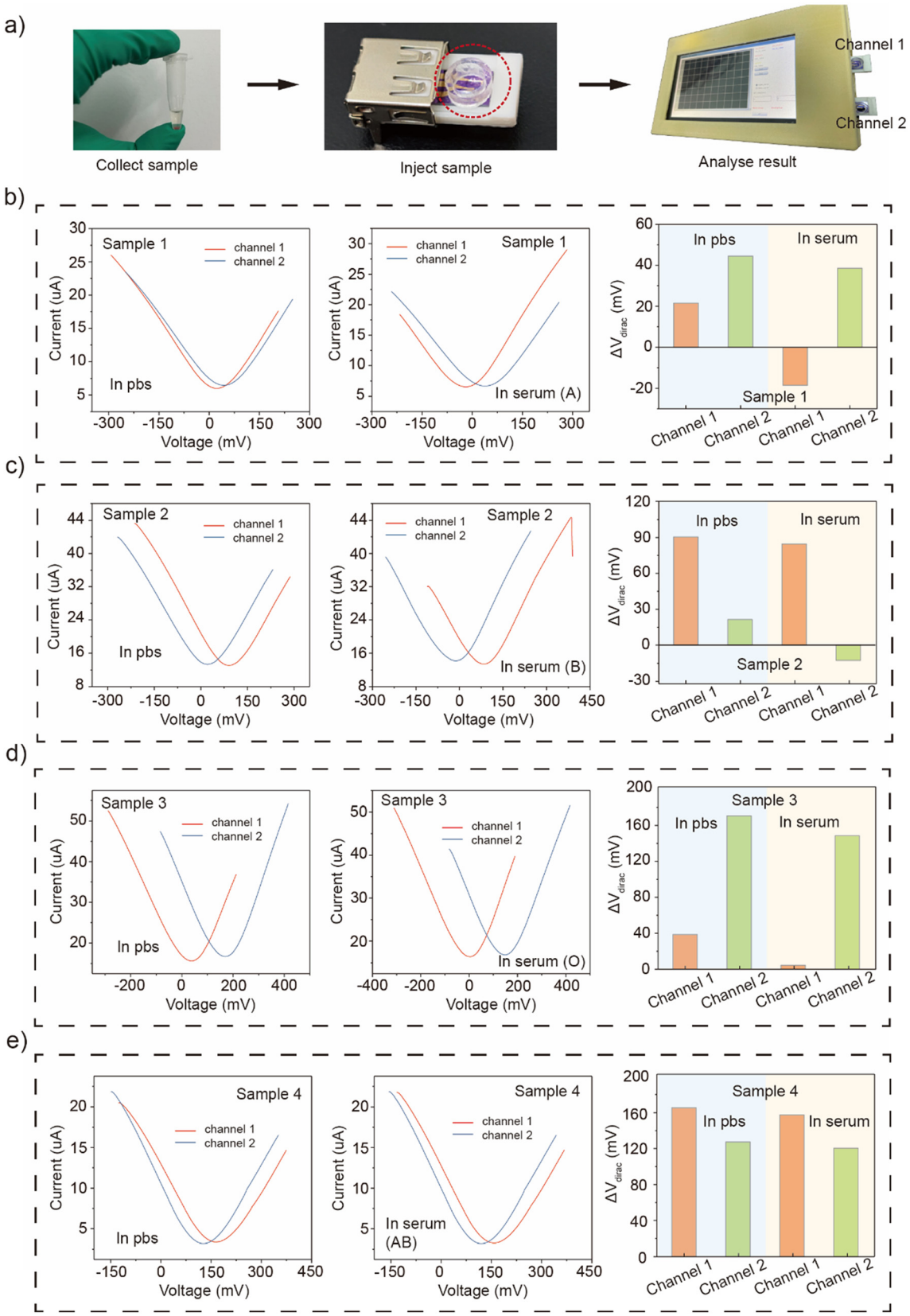

Fig. 5 a) The specific detection steps of C-GFETs for real human blood. b) Illustration of blood type A determination result; c) illustration of blood type B determination result; d) illustration of blood type O determination result; e) illustration of blood type AB determination result.

($\Delta V_{DiracB}/\Delta V_{DiracA}$ = 0.6) served as the boundary between O and AB blood types. Therefore, the criteria for determining blood types are as follows: For a given blood type detection result, if $\Delta V_{DiracB} + \Delta V_{DiracA} < 29$ mV, the blood type can be identified as AB. If $\Delta V_{DiracB} + \Delta V_{DiracA} \geq 29$ mV and $\Delta V_{DiracB}/\Delta V_{DiracA} > 1.6$ (using the upper limit of the standard deviation), the blood type can be identified as A. If $\Delta V_{DiracB} + \Delta V_{DiracA} \geq 29$ mV and $\Delta V_{DiracB}/\Delta V_{DiracA} < 0.6$ (using the lower limit of the standard deviation), the blood type can be identified as B. If $\Delta V_{DiracB} + \Delta V_{DiracA} \geq 29$ mV and $0.6 \leq \Delta V_{DiracB}/\Delta V_{DiracA} \leq 1.6$, the blood type can be identified as O.

3.3. Portable electronic device for ABO blood type detection

To verify whether the portable electronic device could achieve stable voltage output and data acquisition, this paper used a high precise source meter to measure the stepped gate voltage output by the portable device. The device output stepped gate voltages from −500 mV to +500 mV (step size: 10 mV), and the voltage values collected by the source meter and the device itself were plotted for comparison. The results are shown in Fig. 4a. Linear fitting of the gate voltages collected by both devices showed R^2 = 0.9999 for the source meter and R^2 = 1 for the handheld device. The close values indicated that the stepped gate voltage output by the handheld device met the requirements. Additionally, the transfer characteristic curves of the same C-GFET were measured using both the source meter and the electronic device. The results are shown in Fig. 4b.

Finally, the portable electronic device was used to test four types of sera: A, B, AB, and O. The detection process for each blood type consisted of two parts. First, the device's signal response to PBS was measured, and then PBS was replaced with serum for the second measurement. The blood type was determined by comparing the shifts in Dirac point gate voltage between the two measurements.

Fig. 5a shows the structure of the dual-channel C-GFET detection device. And the circuit design is detailed in the SI (Fig. S6). Fig. 5b shows the device's detection results for type A serum. In PBS, the Dirac point gate voltage for channel 1 was $V_{Dirac11}$ = 21.539 mV, and for channel 2, it was $V_{Dirac21}$ = 44.506 mV. After adding serum, the Dirac point values were $V_{Dirac12}$ = −18.513 mV for channel 1 and $V_{Dirac22}$ = 38.577 mV for channel 2. The shifts in Dirac point gate voltage were $\Delta V_{Dirac1} = V_{Dirac11} - V_{Dirac12}$ = 40.502 mV for channel 1 and $\Delta V_{Dirac2} = V_{Dirac21} - V_{Dirac22}$ = 5.929 mV for channel 2. Since $\Delta V_{Dirac1} + \Delta V_{Dirac2}$ = 46.431 mV > 29 mV, the blood type was not AB. Further, $\Delta V_{Dirac1}/\Delta V_{Dirac2}$ = 6.8 > 1.6, so the blood type was identified as A.

Fig. 5c shows the device's detection results for type B serum. $\Delta V_{Dirac1} = V_{Dirac11} - V_{Dirac12}$ = 90.505 − 84.560 = 5.945 mV, $\Delta V_{Dirac2} = V_{Dirac21} - V_{Dirac22}$ = 21.479 − (−12.482) = 33.961 mV. Since $\Delta V_{Dirac1} + \Delta V_{Dirac2}$ = 33.906 mV > 29 mV, the blood type was not AB. Further, $\Delta V_{Dirac1}/\Delta V_{Dirac2}$ = 0.17 < 0.6, so the blood type was identified as B. Fig. 5d shows the device's detection results for type O serum. $\Delta V_{Dirac1} = V_{Dirac11} - V_{Dirac12}$ = 38.529 − 4.487 = 34.042 mV, $\Delta V_{Dirac2} = V_{Dirac21} - V_{Dirac22}$ = 170.608 − (−148.541) = 22.067 mV. Since $\Delta V_{Dirac1} + \Delta V_{Dirac2}$ = 56.109 mV > 29 mV, the blood type was not AB. Further, 0.6 < $\Delta V_{Dirac1}/\Delta V_{Dirac2}$ = 1.54 < 1.6, so the blood type was identified as O. Fig. 5e shows the device's detection results for type AB serum. $\Delta V_{Dirac1} = V_{Dirac11} - V_{Dirac12}$ = 165.594 − (−157.585) = 8.009 mV, $\Delta V_{Dirac2} = V_{Dirac21} - V_{Dirac22}$ = 127.541 − (−120.531) = 7.01 mV. Since $\Delta V_{Dirac1} + \Delta V_{Dirac2}$ = 15.019 mV < 29 mV, the blood type was identified as AB.

4. Conclusions

This paper developed a C-GFET sensing device capable of identifying ABO blood types in real blood samples and developed a portable electronic device to enable routine ABO blood type detection in conjunction with the C-GFET sensing module. The experimental results showed that the sensing system of portable electronic device could specifically and sensitively identify the four common blood types (A, B, AB, O), with the entire detection process completed within 20 minutes. Compared to traditional blood typing methods, the novel sensing system developed in this paper offers advantages such as speed, simplicity, low cost, and ease of portability, holding broad application prospects in clinical point-of-care diagnosis, emergency medicine, rural healthcare services, and personalized medicine.

Author contributions

YL: conceptualisation, data curation, formal analysis, investigation, methodology, validation, visualisation, writing original draft, writing – review & editing; PL: resources, supervision, writing – review & editing; YY: investigation, writing – review & editing; WZ: conceptualisation, formal analysis, funding acquisition, methodology, project administration, writing – original draft.

Conflicts of interest

There are no conflicts to declare.

Data availability

The data presented in this study are available on request from the corresponding author.

References

1 A. Cossarizza, H. Chang, A. Radbruch, S. Abrignani, R. Addo, M. Akdis, I. Andrä, F. Andreata, F. Annunziato, E. Arranz, P. Bacher, S. Bari, V. Barnaba, J. Barros-Martins, D. Baumjohann, C. G. Beccaria, D. Bernardo, D. A. Boardman, J. Borger, C. Böttcher, L. Brockmann, M. Burns, D. H. Busch, G. Cameron, I. Cammarata, A. Cassotta, Y. Chang, F. G. Chirdo, E. Christakou, L. Čičin-Šain, L. Cook, A. J. Corbett, R. Cornelis, L. Cosmi, M. S. Davey, S. De Biasi, G. De Simone, G. Del Zotto, M. Delacher, F. Di Rosa, J. Di Santo, A.

Diefenbach, J. Dong, T. Dörner, R. J. Dress, C. Dutertre, S. B. G. Eckle, P. Eede, M. Evrard, C. S. Falk, M. Feuerer, S. Fillatreau, A. Fiz-Lopez, M. Follo, G. A. Foulds, J. Fröbel, N. Gagliani, G. Galletti, A. Gangaev, N. Garbi, J. A. Garrote, J. Geginat, N. A. Gherardin, L. Gibellini, F. Ginhoux, D. I. Godfrey, P. Gruarin, C. Haftmann, L. Hansmann, C. M. Harpur, A. C. Hayday, G. Heine, D. C. Hernández, M. Herrmann, O. Hoelsken, Q. Huang, S. Huber, J. E. Huber, J. Huehn, M. Hundemer, W. Y. K. Hwang, M. Iannacone, S. M. Ivison, H. Jäck, P. K. Jani, B. Keller, N. Kessler, S. Ketelaars, L. Knop, J. Knopf, H. Koay, K. Kobow, K. Kriegsmann, H. Kristyanto, A. Krueger, J. F. Kuehne, H. Kunze-Schumacher, P. Kvistborg, I. Kwok, D. Latorre, D. Lenz, M. K. Levings, A. C. Lino, F. Liotta, H. M. Long, E. Lugli, K. N. MacDonald, L. Maggi, M. K. Maini, F. Mair, C. Manta, R. A. Manz, M. Mashreghi, A. Mazzoni, J. McCluskey, H. E. Mei, F. Melchers, S. Melzer, D. Mielenz, L. Monin, L. Moretta, G. Multhoff, L. E. Muñoz, M. Muñoz-Ruiz, F. Muscate, A. Natalini, K. Neumann, L. G. Ng, A. Niedobitek, J. Niemz, L. N. Almeida, S. Notarbartolo, L. Ostendorf, L. J. Pallett, A. A. Patel, G. I. Percin, G. Peruzzi, M. Pinti, A. G. Pockley, K. Pracht, I. Prinz, I. Pujol-Autonell, N. Pulvirenti, L. Quatrini, K. M. Quinn, H. Radbruch, H. Rhys, M. B. Rodrigo, C. Romagnani, C. Saggau, S. Sakaguchi, F. Sallusto, L. Sanderink, I. Sandrock, C. Schauer, A. Scheffold, H. U. Scherer, M. Schiemann, F. A. Schildberg, K. Schober, J. Schoen, W. Schuh, T. Schüler, A. R. Schulz, S. Schulz, J. Schulze, S. Simonetti, J. Singh, K. M. Sitnik, R. Stark, S. Starossom, C. Stehle, F. Szelinski, L. Tan, A. Tarnok, J. Tornack, T. I. M. Tree, J. J. P. Van Beek, W. Van De Veen, K. Van Gisbergen, C. Vasco, N. A. Verheyden, A. Von Borstel, K. A. Ward-Hartstonge, K. Warnatz, C. Waskow, A. Wiedemann, A. Wilharm, J. Wing, O. Wirz, J. Wittner, J. H. M. Yang and J. Yang, Guidelines for the use of flow cytometry and cell sorting in immunological studies (third edition), *Eur. J. Immunol.*, 2021, **51**, 2708–3145.

2 H. C. Ates, J. A. Roberts, J. Lipman, A. E. G. Cass, G. A. Urban and C. Dincer, On-site therapeutic drug monitoring, *Trends Biotechnol.*, 2020, **38**, 1262–1277.

3 J. Saunders, I. A. P. Thompson and H. T. Soh, Generalizable molecular switch designs for *in vivo* continuous biosensing, *Acc. Chem. Res.*, 2025, **58**, 703–713.

4 F. Ricci and G. Palleschi, Sensor and biosensor preparation, optimisation and applications of prussian blue modified electrodes, *Biosens. Bioelectron.*, 2005, **21**, 389–407.

5 A. K. Yetisen, J. L. Martinez-Hurtado, B. Ünal, A. Khademhosseini and H. Butt, Wearables in medicine, *Adv. Mater.*, 2018, **30**, 1706910.

6 T. Huo, F. Li, K. Jiang, W. Kong, X. Zhao, Z. Hao and Y. Pan, Fluorocarbon-based selective-superwetting nanofibrous membranes with ultraviolet-driven switchable wettability for oil–water separation, *ACS Appl. Nano Mater.*, 2022, **5**, 13018–13026.

7 P. Miao and Y. Tang, Cascade toehold-mediated strand displacement reaction for ultrasensitive detection of exosomal MicroRNA, *CCS Chem.*, 2021, **3**, 2331–2339.

8 P. Miao and Y. Tang, Cascade toehold-mediated strand displacement reaction for ultrasensitive detection of exosomal MicroRNA, *CCS Chem.*, 2021, **3**, 2331–2339.

9 B. Unnikrishnan, S. Palanisamy and S.-M. Chen, A simple electrochemical approach to fabricate a glucose biosensor based on graphene–glucose oxidase biocomposite, *Biosens. Bioelectron.*, 2013, **39**, 70–75.

10 D. Bizzotto, I. J. Burgess, T. Doneux, T. Sagara and H.-Z. Yu, Beyond simple cartoons: challenges in characterizing electrochemical biosensor interfaces, *ACS Sens.*, 2018, **3**, 5–12.

11 H. Wang, Z. Hao, C. Huang, F. Li and Y. Pan, Monitoring Cd^{2+} in oily wastewater using an aptamer-graphene field-effect transistor with a selective wetting surface, *Nanoscale Adv.*, 2023, **5**, 1416–1424.

12 Z. Hao, X. Fang, Z. Wang, C. Huang, F. Li, Y. Luo, Y. Ying, S. Ma, Y. Jia, X. Wang and Y. Pan, Intelligent wearable graphene nano-electronics with switchable surface wettability capabilities for autonomous sweat enrichment-purification-analysis, *Adv. Funct. Mater.*, 2024, **34**, 2400947.

13 U. Latif, A. Seifner and F. L. Dickert, Selective detection of erythrocytes with QCMs—ABO blood group typing, *Sens.*, 2023, **23**, 7533.

14 K. Nanameki, H. Ushijima, S. Akase, T. Matsumoto and S. Kamata, The rapid measurement of ABO blood type by using surface-plasmon resonance sensor, *Bunseki Kagaku*, 1999, **48**, 669–672.

15 K. Sode and J. Kerrigan, Elucidating the mechanism of electrochemical inactivation of direct electron transfer type glucose dehydrogenase enzyme-employing biosensor, *ECS Meet. Abstr.*, 2024, **MA2024-2**, 3652.

16 R. Escalona-Villalpando, A. Sandoval-García, J. Espinosa-Lumbreras, M. Miranda-Silva, L. Arriaga, S. D. Minteer and J. ledesma-García, Design and Evaluation of a Microfluidic Device Such As a Self-Powered Glucose Biosensor Using a Solution of Glucose and Human Blood, *ECS Meet. Abstr.*, 2022, **MA2022-1**, 2188.

17 D. H. Ho, Q. Sun, S. Y. Kim, J. T. Han, D. H. Kim and J. H. Cho, Stretchable and multimodal all graphene electronic skin, *Adv. Mater.*, 2016, **28**, 2601–2608.

18 B. H. Nguyen and V. H. Nguyen, Promising applications of graphene and graphene-based nanostructures, *Adv. Nat. Sci.: Nanosci. Nanotechnol.*, 2016, **7**, 23002.

19 H. Jiang, Chemical preparation of graphene-based nanomaterials and their applications in chemical and biological sensors, *Small*, 2011, **7**, 2413–2427.

20 G. Speranza, Carbon nanomaterials: synthesis, functionalization and sensing applications, *Nanomaterials*, 2021, **11**, 967.

21 X. Chen, D. Wang, W. Ding, H. Zang and L. Li, Single-walled carbon nanotubes sensors: preparation and bio-application advances, *Pharm. Sci. Adv.*, 2025, **3**, 100064.

22 Q. Huang, X. Lin, L. Tong and Q.-X. Tong, Graphene quantum dots/multiwalled carbon nanotubes composite-based electrochemical sensor for detecting dopamine release from living cells, *ACS Sustainable Chem. Eng.*, 2020, **8**, 1644–1650.

23 Z. Qian, X. Shan, L. Chai, J. Ma, J. Chen and H. Feng, Si-doped carbon quantum dots: a facile and general preparation strategy, bioimaging application, and multifunctional sensor, *ACS Appl. Mater. Interfaces*, 2014, **6**, 6797–6805.
24 Z. Štukovnik, R. Fuchs-Godec and U. Bren, Nanomaterials and their recent applications in impedimetric biosensing, *Biosensors*, 2023, **13**, 899.
25 R. Kour, S. Arya, S.-J. Young, V. Gupta, P. Bandhoria and A. Khosla, Review—recent advances in carbon nanomaterials as electrochemical biosensors, *J. Electrochem. Soc.*, 2020, **167**, 37555.
26 F. Sher, I. Ziani, M. Smith, G. Chugreeva, S. Z. Hashimzada, L. D. T. Prola, J. Sulejmanović and E. K. Sher, Carbon quantum dots conjugated with metal hybrid nanoparticles as advanced electrocatalyst for energy applications – a review, *Coord. Chem. Rev.*, 2024, **500**, 215499.
27 A. Walcarius, S. D. Minteer, J. Wang, Y. Lin and A. Merkoçi, Nanomaterials for bio-functionalized electrodes: recent trends, *J. Mater. Chem. B*, 2013, **1**, 4878.
28 Y. Zhang, G. Figueroa-Miranda, C. Zafiu, D. Willbold, A. Offenhäusser and D. Mayer, Amperometric aptasensor for amyloid-β oligomer detection by optimized stem-loop structures with an adjustable detection range, *ACS Sens.*, 2019, **4**, 3042–3050.
29 T. Huo, X. Xue, Y. Sun, S. Huang, Y. Pan and F. Li, Glomerulus inspired charged nanofibrous membrane for high-efficient micro/nano-emulsion separation, *Adv. Funct. Mater.*, 2026, e21336.
30 A. R. Minerick, The rapidly growing field of micro and nanotechnology to measure living cells, *AIChE J.*, 2008, **54**, 2230–2237.
31 H. Qadir, M. O. Larik and M. A. Iftekhar, Bombay blood group phenotype misdiagnosed As O phenotype: a case report, *Cureus*, 2023, **15**, e45555.
32 S. Gabaidze, M. Nagervadze, L. Akhvlediani, N. Nakashidze, A. Alfilo, I. Tsintsadze, N. Gorgadze, R. Khukhunaishvili, M. Koridze, T. Koiava, K. Dolidze and T. Bakhtadze, ABO and Rh blood group antigens and natural anti-a and ANTI-B antibodies in the neonates, *WSEAS Trans. Biol. Biomed.*, 2023, **20**, 186–196.
33 U. Galili, J. Buehler, S. B. Shohet and B. A. Macher, The human natural anti-gal IgG. III. The subtlety of immune tolerance in man as demonstrated by crossreactivity between natural anti-gal and anti-B antibodies, *J. Exp. Med.*, 1987, **165**, 693–704.
34 B. Sowa and M. Kunysz, Interference of anti-M antibody with ABO blood grouping — own experience, *J. Transfus. Med.*, 2024, **17**, 1–6.